

Transient melting of an ESR electrode

This content has been downloaded from IOPscience. Please scroll down to see the full text.

2016 IOP Conf. Ser.: Mater. Sci. Eng. 143 012003

(<http://iopscience.iop.org/1757-899X/143/1/012003>)

View [the table of contents for this issue](#), or go to the [journal homepage](#) for more

Download details:

IP Address: 193.170.16.107

This content was downloaded on 22/09/2016 at 09:49

Please note that [terms and conditions apply](#).

You may also be interested in:

[Electrochemical Aspects of the ESR Process](#)

Alec Mitchell

[Nuclear reactions in the storage ring ESR with EXL](#)

Th Kröll, M von Schmid, J C Zamora et al.

[Forward-angle electron spectroscopy in heavy-ion atom collisions studied at the ESR](#)

P-M Hillenbrand, S Hagmann, Yu A Litvinov et al.

[ESR Measurements at Temperatures around 0.1 K](#)

Hidetaro Abe and Kei-ichi Koga

[Electron spin resonance in spin-gap compounds with bond randomness](#)

Hirotaaka Manaka

[ESR of Photodarkened CdS-Doped and Undoped Glasses](#)

Tadaki Miyoshi, Ken-ichi Towata and Naoto Matsuo

[Development and application of high field and high pressure ESR system](#)

T Sakurai, A Taketani, T Tomita et al.

Transient melting of an ESR electrode

A Kharicha^{a,b}, E Karimi-Sibaki^a, J Bohacek^b, M Wu^{a,b}, and A Ludwig^b

^aChristian-Doppler Lab for Adv. Process Simulation of Solidification & Melting,

^bChair of Simulation and Modeling of Metallurgical Processes,
University of Leoben, Franz-Josef-Str. 18, A-8700 Leoben, Austria

E-mail: abdellah.kharicha@unileoben.ac.at

Abstract. Melting parameters of ESR process such as melt rate and immersion depth of electrode are of great importance. In this paper, a dynamic mesh based simulation framework is proposed to model melt rate and shape of electrode during the ESR process. Coupling interactions between turbulent flow, temperature, and electromagnetic fields are fully considered. The model is computationally efficient, and enables us to directly calculate melting parameters. Furthermore, dynamic change of electrode shape by melting can be captured. It is necessary to control the feeding velocity of electrode due to melting instabilities in the ESR process. As such, a numerical control is implemented based on the immersion depth of electrode to achieve the steady state in the simulation. Furthermore, the modeling result is evaluated against an experiment.

1. Introduction

The electroslag remelting (ESR) process is used for manufacture of superior quality steel and super alloys such as titanium alloys. Within the process, a consumable electrode melts through an electrically resistive slag layer through Joule heating. Then, droplets from the electrode pass through the slag and reach the liquid melt pool. Finally, the melt pool solidifies in a water-cooled mold to build the high-grade ingot. The internal quality of ingot is characterized according to the shape of melt pool especially depth and thickness of mushy zone. A shallow melt pool is favorable to achieve unidirectional solidification. Furthermore, producing an ingot with a defect-free surface is desirable. The electrode melt rate is a key parameter, affecting internal and surface quality of ingot. The influence of melt rate on the pool shape of an ESR ingot was investigated by Mitchell [1]. The depth of melt pool and thickness of the mushy zone were found to increase when the process was operated with higher melt rate. However, Suarez [2] reported that with the increase of melt rate a relatively smooth ingot surface can be obtained.

As reported by Kishida et al. [3], the melt rate, shape and immersion depth of electrode are interdependent parameters that are significantly influenced by the amount of power generated in the process. With the increase of voltage (generated power) in the process, the following melting behaviors were observed: the melt rate increases, the immersion depth decreases, and the shape of electrode tip becomes flatter. Over the last decades, a number of studies were carried out on this topic. For instance, Mitchell et al. modeled the temperature field in the electrode for a laboratory scale ESR process [4]. Their calculated temperature profile agreed with the experimental result. Mendrykowski et al, found that thermal radiation on the surface is ignorable compared to heat conduction along the electrode [5]. Tacke et al. [6] conducted a series of experiments to investigate melting behavior of a laboratory scale ESR electrode. Furthermore, they proposed an approximate formula for the immersion depth which was validated against experiments. By evaluation of thermal fluxes through



boundaries, Jardy et al. predicted higher melt rate when buoyancy force is stronger than electromagnetic force [7]. Yanke et al. applied an effective heat transfer coefficient to study the melting behavior of an industrial scale ESR process [8]. Recently, Kharicha et al [9] modeled electrode melting within the framework of multiphase Volume of Fluid (VOF) method. It was stated that the coupling between melt rate and Joule heat is very unstable. Details of flow, temperature, and magnetic field during electrode melting were described. However, the proposed VOF based method is computationally expensive.

In this paper, a dynamic mesh-based simulation framework is proposed to model melting and shape of electrode tip. The proposed method is robust and computationally efficient. Complex interactions between flow, temperature, and electromagnetic fields are considered. In ESR process, it is necessary to continuously track and control immersion depth of electrode due to melting instability. In order to achieve stability in the simulation, a numerical control of immersion depth is implemented. Details of flow, temperature, and electromagnetic fields during remelting are demonstrated. Furthermore, the model is evaluated against experimental results [6].

2. A brief description of the model

Previously, the governing equations of flow, heat, and electromagnetic fields together with related boundary conditions as well as simulation parameters such as material properties and operation conditions were presented in details [10]. Here, a short description of the model is given. An axisymmetric computational domain is considered including electrode, slag, air, mold, and liquid zones as shown in Figure 1 (a). The Finite Volume Method (FVM) is used to simulate fluid flow, heat transfer, and electromagnetic fields. The commercial CFD software, FLUENT-ANSYS v.14.5, is the solver that includes a dynamic mesh technique for the simulation of displacements of boundaries. The modeling equations for fields such as electromagnetic field or boundaries (stationary and moving) are implemented using User-Defined Functions (UDF).

The well-known $A-\phi$ formulation is used to compute the electromagnetic field where ϕ is the electric scalar potential and A denotes the magnetic vector potential. After calculating the magnetic field and subsequently electric current density distribution, the Lorentz force as well as Joule heating are obtained and added as source terms to momentum and energy equations respectively. Applying $A-\phi$ formulation to calculate electromagnetic field was extensively described by Kharicha [9].

The turbulent flow field in slag and melt pool is calculated considering the effect of Lorentz force and thermal buoyancy (Boussinesq approximation). The turbulence in the system is modeled using SST- $k-\omega$ approach. The essential feature of SST model is an accurate and effective near wall treatment due to insensitivity of the model to grid spacing of near wall cells [11-12]. The enthalpy conservation equation is solved to determine the temperature field taking into accounts Joule heating and latent heat sink (S_{LH}) required to melt the electrode [10, 13]. The latter will be described after introducing equations regarding to displacement of boundaries (electrode tip-slag and slag-air interfaces).

Displacements of domain boundaries are modeled using dynamic and deformable meshes in which the mesh nodes can be relocated. The following dynamic mesh schemes are used to handle boundary movement in the system. Firstly, layering scheme is used that involves creation and destruction of cell rows in the vicinity of a moving boundary. Secondly, smoothing scheme is applied in which the grid nodes are considered as a network of interconnected springs. The connectivity between grid nodes remains unchanged, but they can reposition [14]. In the computational domain, slag-air interface (moving) and electrode tip (moving-deforming) boundaries are allowed to move as shown in Figure 1(b). A high resolution mesh with equisized cells is used in the whole domain with the total number of 20000 cell elements (the mesh resolution is shown in melt pool).

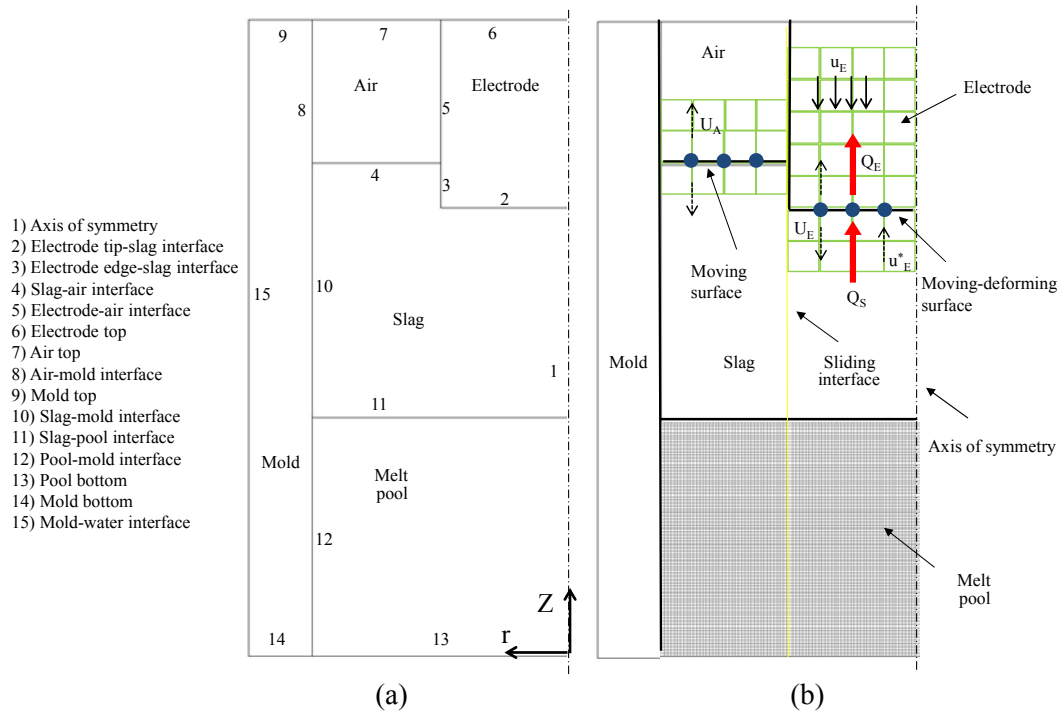


Figure 1. (a) Configuration of computational domain and boundaries, (b) Conceptual demonstration of heat balances across the electrode tip, melting velocity, feeding velocity, total velocity, and slag-air interface velocity (Note that the mesh resolution is very fine with equisized cells in the whole domain that is shown in melt pool, however the mesh is exaggeratedly shown to be coarse near the electrode for illustrative purpose)

Note that, both temperature field of electrode and velocity of melting at electrode tip are unknown. Physically, no dendritic mushy zone was observed during melting process, and the liquid-solid interface remained smooth. As such, melting of electrode can be considered as a Stefan problem where a phase boundary moves with time. The velocity of grid nodes at moving boundaries are computed using a set of balances equations. The velocity of dynamically deforming electrode tip is determined according to the amount of heat provided to the electrode through the slag.

$$U_E = u_E^* - u_E \quad (1)$$

$$Q_S - Q_E = \rho_{metal} \Delta H u_E^* \quad (2)$$

$$\begin{cases} u_E^* \geq 0 & (Q_S > Q_E) \\ u_E^* < 0 & (Q_S < Q_E) \end{cases} \quad (3)$$

According to Eq. (1), the grid node velocity of the electrode tip (U_E) is the sum of melting velocity (u_E^*) and the electrode feeding velocity (u_E). Based on Eq. (2), the melting velocity is dependent on the heat flux provided to the electrode (Q_S), heat flux diffused into the electrode (Q_E), density of metal ($\rho_{metal} \sim 7100 \text{ kg.m}^{-3}$), and the latent heat of fusion ($\Delta H \sim 260 \text{ kJ.kg}^{-1}$). The origin of z-referential is set at the bottom of computational domain. Therefore, the sign (positive or negative) of melting velocity

depends on the balance of heat fluxes at the electrode tip as expressed in Eq. (3). Consider that, the right hand side of Eq. (2) describes the amount of latent heat provided to melt the electrode. Therefore, the volumetric source of latent heat (S_{LH}) that is absorbed adjacent to electrode tip is given by

$$S_{LH} = \rho_{metal} u_E^* \Delta H \left(\frac{S_{cell-electrode}}{V_{cell-electrode}} \right) \quad (4)$$

where ($S_{cell-electrode}$) denotes the face area of a cell that belongs to the electrode tip and ($V_{cell-electrode}$) is the cell volume.

With the increase of electrode immersion depth, the slag level rises to conserve the total mass of slag. Therefore, the slag-air interface is also modeled as a moving boundary. The velocity of grid nodes (U_A) of the slag-air moving boundary is computed as:

$$U_A = \frac{m_0 - m}{\rho_{slag} \Delta t \pi (R_{mold}^2 - R_{electrode}^2)} \quad (5)$$

where (m_0) denotes the slag initial mass, (m) is the computed mass, ($\rho_{slag} \sim 2700 \text{ kg.m}^{-3}$) is density of slag, ($\Delta t \sim 0.1 \text{ s}$) is time step size, and (R_{mold}) and ($R_{electrode}$) are the radius of the mold and electrode respectively.

The electrode feeding velocity is preferred to be kept constant during industrial operation of an ESR process. It is necessary to adapt feeding velocity (u_E) according to the immersion depth to stabilize the electrode position so that the electrode tip neither reaches the melt pool nor the slag free surface [9]. The following restriction is imposed on the feeding velocity of electrode:

$$u_E = u_E^0 \min \left[1, \frac{l_{max} - l}{l_{max} - l_{min}} \right] \quad (6)$$

(l_{min}) and (l_{max}) are minimum and maximum allowable immersion depth of electrode, and (u_E^0) is initial feeding velocity which are the input parameters of the process. Furthermore, a uniform velocity field inside the electrode zone is specified which has similar magnitude as the electrode feeding velocity (u_E).

The simulation is executed in transient where the immersion depth and shape of electrode tip is continuously tracked. The steady state is achieved once the velocity of grid nodes (U_E) converges to zero. The melt rate ($\dot{m} \geq 0$) of electrode can be directly computed as follow:

$$\dot{m} = -\rho_{metal} \iint_{S_{electrode}} \vec{u}_E^* \cdot d\vec{S} \quad (7)$$

Following the experiment of Tacke [6] on a laboratory scale ESR process, we used an identical geometry and operating parameters. Table 1 lists the parameters used in the experiment [6] and our simulation. Furthermore, the steady state melting parameters of simulation such as computed immersion depth are listed.

Table 1. Operation conditions and results of a laboratory scale ESR process [6], a comparison is also made with the simulation results (steady state).

	Experiment [6]	Simulation
Electric current mode	DC	DC
Electric current (kA)	1.9	1.9
Mold current	Unknown	Yes
Electrode radius (cm)	4	4
Mold radius (cm)	8	8
Slag weight (kg)	4.0	4.1
Slag electric cond. ($\text{ohm}^{-1}.\text{m}^{-1}$)	Unknown	150
Slag thermal cond. ($\text{W}.\text{m}^{-1}.\text{K}^{-1}$)	Unknown	4
Slag therm. exp. coeff. (K^{-1})	Unknown	9×10^{-5}
Voltage (V)	29	28
Power (kW)	55	57
Initial feeding vel. ($\text{cm}.\text{s}^{-1}$)	Unknown	0.0153
Steady feeding vel. ($\text{cm}.\text{s}^{-1}$)	0.0153	0.0076
Melt rate ($\text{g}.\text{s}^{-1}$)	5.5	3.7
Immersion depth (cm)	3.8	3.56
L_{\min} (cm)	Unknown	2.5
L_{\max} (cm)	Unknown	4.5

It must be noted that the following phenomena are not considered in our model. As generally recognized, the electric current is conducted by ions in the slag region. Consequently, difference in melt rate is observed based on the polarity of electrode (positive or negative) due to polarization overpotential [15]. Formation of a liquid film under the electrode and dripping of droplets through the slag are also not included [16-17]. Solidification of liquid pool is also ignored.

3. Results and discussions

A constant magnitude of DC current is imposed in the process. Additionally, it is assumed that the current can cross the slag skin flowing through the mold [15, 18-19]. The initial feeding velocity is not reported for the experiment, but the steady feeding velocity is known. Furthermore, the feeding velocity is adjusted adapted by Eq. 6 in the simulation. Figure 2 illustrates the evolution of electrode shape including electric potential, velocity, and temperature fields in slag and submerged part of the electrode. The amplitude of voltage drop and power generated in the system depends on immersion depth (indicated by the distance between electrode tip and isolines of voltage drop). Decreasing immersion depth leads to significant voltage drop and power generation in the system as shown in Figure 2 (c). Therefore, the temperature notably elevates in the bulk of slag. With the increase of immersion depth, the isolines of voltage are shifted and the total voltage in the system decreases. However, the current density increases in the central region of slag and subsequently the Lorentz force become stronger. The latter intensifies the velocity under the shadow of electrode which results in promotion of stirring in the slag zone that is shown in Figure 2 (e). Here, the global energy transport is efficient due to strong turbulence which causes relatively uniform slag temperature. Finally, electrode develops a conical shape at steady state ($t = 350$ s). The mesh resolution near moving-deforming boundary (electrode tip) is also shown in Figure 2. Accordingly, the quality of mesh is very well preserved.

The variation in melt rate and generated power as well as feeding velocity and immersion depth are plotted during deformation of electrode tip until reaching the steady state which is shown in Figure 3. The results show that variation in generated power is much smoother than melt rate. The peak observed in generated power indicates the situation where the immersion depth is very shallow.

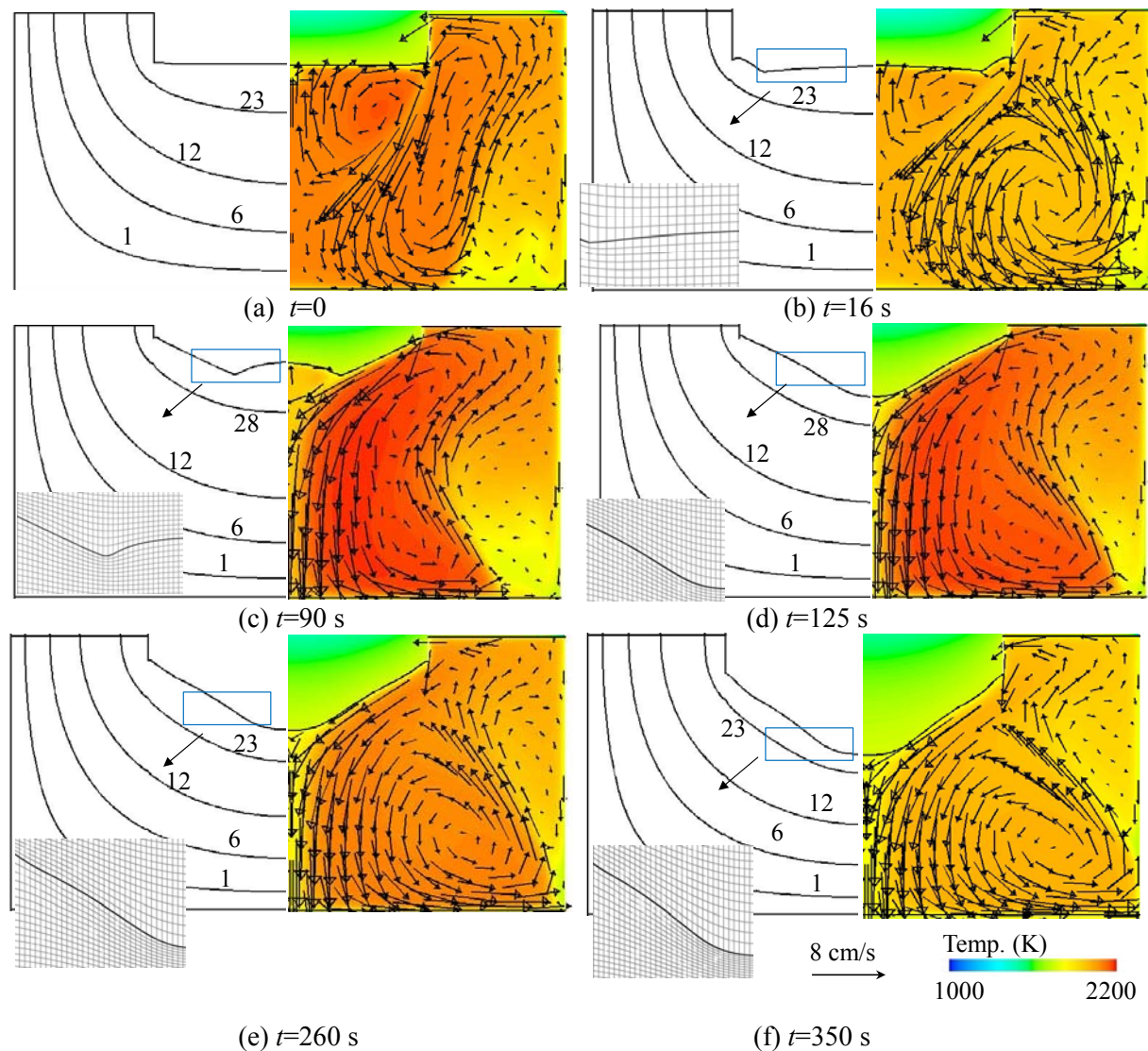


Figure 2. Evolution of shape of electrode tip: (a) $t=0$, (b) $t=16$ s, (c) $t=90$ s, (d) $t=125$ s, (e) $t=260$ s, (f) $t=350$ s. On left half: isolines of voltage, and the grid node near the moving boundary (electrode tip). On right half: contour of temperature overlaid with the vectors of velocity in the slag region.

Despite gentle variation in generated power, the melt rate can dramatically increase or decrease before reaching the steady state. In fact, the melt rate is governed by the amount of heat provided to the electrode which is highly influenced by complex interactions between flow, temperature, and electromagnetic fields. For example, with decrease of immersion depth, Figure 3 (d), the generated power increases, Figure 3 (a) that leads to hotter slag and increase of melt rate as shown in Figure 2 (c). Furthermore, the constraint imposed on the immersion depth based on Eq. 6 can certainly affect the feeding velocity as well as melt rate of electrode. Further investigation is required to explore the effect of immersion depth control on melting behavior of electrode that is beyond the scope of the current work. Figure 4 compares the experimentally observed shape of electrode with the predicted shape in the simulation at steady state where a relatively good agreement is obtained. In any case, the shape of electrode tip is mainly influenced by temperature and flow distribution which are highly dependent on slag properties. The slag properties are temperature dependent, so a large uncertainty on the reported values exists due to difficulty of measurements at high temperature. For instance, the

thermal conductivity of slag was reported to vary between 1 to 5 $\text{W.m}^{-1}.\text{K}^{-1}$, whereas the electrical conductivity was measured to be between 80 to 300 $\text{ohm}^{-1}.\text{m}^{-1}$ [20-21].

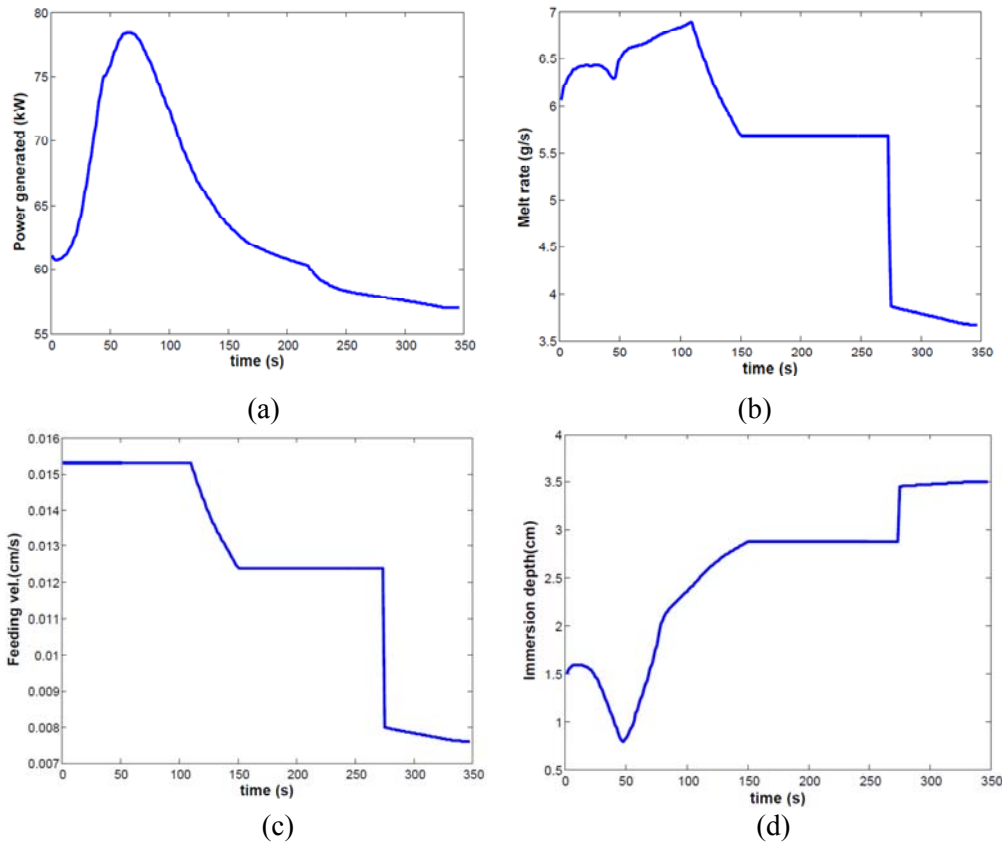


Figure 3. Analysis of melting parameters: (a) generated power, (b) melt rate of electrode, (c) feeding velocity, (d) immersion depth.

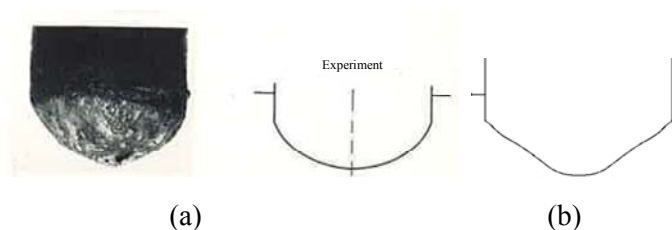


Figure 4. A comparison of (a) the shape of electrode tip as observed in the experiment [6] with (b) the calculated shape of electrode from simulation.

It must be reported that we ran many simulations to perform a parameter study to investigate the effect of slag physicochemical properties such as electrical and thermal conductivity on the melt rate and shape of electrode. Our investigations were published with details in the previous paper [10]. It must be stated that the predicted melt rate by the simulation is lower than the value reported in experiment [Table 1]. The current model does not take into account effects of electrochemical reactions, formation of liquid film at electrode tip and dripping of droplets through slag. In fact departure and dripping of droplets can create stronger turbulence which enhance global energy transfer and melt rate of electrode [16-17]. The aforementioned phenomena must be included in the future model to improve quantitative accuracy of the model.

4. Summary

A dynamic mesh based approach is used to model submerging and remelting of electrode in electroslag remelting (ESR) process. The computational domain is 2D axisymmetric where interactions between turbulent flow, temperature, and electromagnetic fields are fully taken into account. It is shown that the model is capable of predicting the evolution of electrode shape during remelting. In order to achieve steady state, the immersion depth of electrode is continuously tracked and controlled. For the latter, a numerical control of feeding velocity is implemented dependent on the immersion depth. The model is computationally robust that enables us to directly compute melt rate without using any further assumption (e.g. heat transfer coefficient between electrode-slag). The shape of electrode is also validated against the experiment. Melt rate and shape of electrode are highly dependent on physicochemical properties of slag such as thermal and electrical conductivities. The effect of slag properties on melting behavior of electrode is extensively discussed in other paper [10].

5. Acknowledgement

The authors acknowledge the financial support by the Austrian Federal Ministry of Economy, Family and Youth and the National Foundation for Research, Technology and Development within the framework of the Christian Doppler Laboratory for Advanced Process Simulation of Solidification and Melting.

6. References

- [1] Mitchell A 1984 *Conf. on Perspective in Metallurgical Development* (Sheffield) p 89
- [2] Suarez F S, Roberts J E, and Schley L.D 1974 *5th Int. Symp. on Electroslag and Other Special Melting Technologies* (Pittsburgh) p 126
- [3] Kishida T, Yamaguchi T, Tomioka T, and Ichihara T 1974 *Elect. steel* **45** 219
- [4] Mitchell A, Joshi S, and Cameron J 1971 *Metall. Trans.* **2** 561
- [5] Mendrykowski J, Poveromo J, Szekely J, and Mitchell A 1972 *Metall. Trans.* **4** 1761
- [6] Tacke K H and Schwerdtfeger K 1981 *Arch. Eisenhüttenwesen* **52** 137
- [7] Jardy A, Ablitzer D, Wadier J F 1991 *Metall. Trans.* **22** 111
- [8] Yanke J, Fezi K, Fahrman M, and Krane M J M 2013 *Proc. Of LMPC* (New York: Wiley–Interscience)
- [9] Kharicha A, Wu M, and Ludwig A 2014 *ISIJ* **54** 1621
- [10] Karimi-Sibaki E, Kharicha A, Bohacek J, Wu M, and Ludwig A, *Metall. Mater. Trans. B*, DOI 10.1007/s11663-015-0384-0
- [11] Menter F R 1994 *AIAA Journal* **32** 1598
- [12] Menter F R, Kuntz M, and Langtry R 2003 *Turb. Heat and Mass Trans.* **4** 625
- [13] Karimi-Sibaki E, Kharicha A, Korp J, Wu M, Ludwig A 2014 *Mater. Sci. Forum* **790** 396
- [14] Fluent 14.5 user's guide 2012 (Austin: Fluent Inc.)
- [15] Kawakami M, Nagata K, Yamamura M, Sakata N, Miyashita Y, and Goto K S 1977 *Testsu-to-Hagane* **63** 220
- [16] Kharicha A, Ludwig A, and Wu M 2011 *EPD congress* (San Diego) p 771
- [17] Kharicha A, Wu M, Ludwig A, Ramprecht M, Holzgruber H 2012 *CFD modeling and simulation in materials* (New York: Wiley–Interscience) p 139
- [18] Kharicha A, Ludwig A, and Wu M. 2005 *Mater. Sci. Eng. A* **413** 129
- [19] Kharicha A, Schutzenhofer W, Ludwig A, Tanzer R, and Wu M 2008 *Steel Res. Int.* **79** 632
- [20] Taylor R, Mills K C 1982 *Arch. Eisenhüttenwesen* **53** 55
- [21] Hajduk M and Gammal T E 1979 *Stahl Eisen* **99** 113